Journal of Hazardous Materials 498 (2025) 139885

Contents lists available at ScienceDirect

Journal of Hazardous Materials

journal homepage: www.elsevier.com/locate/jhazmat

# Application of multi-dimensional isotope fractionation to characterize the biotic and abiotic transformation mechanisms of the herbicide 2,4-dichlorophenoxyacetic acid

Jukun Xiong [a,b,*], Yongyu Liang [a,b], Chang Yuan [a,b], Suyun Chen [a,b], Meicheng Wen [a,b], Wanjun Wang [a,b], Qinhao Lin [a,b], Yingxin Yu [a,b]

[a] Guangdong Key Laboratory of Environmental Catalysis and Health Risk Control, Guangdong-Hong Kong-Macao Joint Laboratory for Contaminants Exposure and Health, Institute of Environmental Health and Pollution Control, Guangdong University of Technology, Guangzhou 510006, China
[b] Guangdong Basic Research Center of Excellence for Ecological Security and Green Development, Guangdong Technology Research Center for Photocatalytic Technology Integration and Equipment Engineering, School of Environmental Science and Engineering, Guangdong University of Technology, Guangzhou 510006, China

## HIGHLIGHTS

- Multi-element isotope analysis characterizes underlying reaction mechanism of 2,4-D.
- H-abstraction reaction was the main rate-limiting step for 2,4-D biodegradation.
- Cleavage of C-O bond was dominant rate-limiting step for 2,4-D photodegradation.
- Multiple isotope fractionations distinguish C-O bond cleavage for the first time.
- 2,4-Dichloropheol was the common main product for both biotic and abiotic pathways.

## GRAPHICAL ABSTRACT

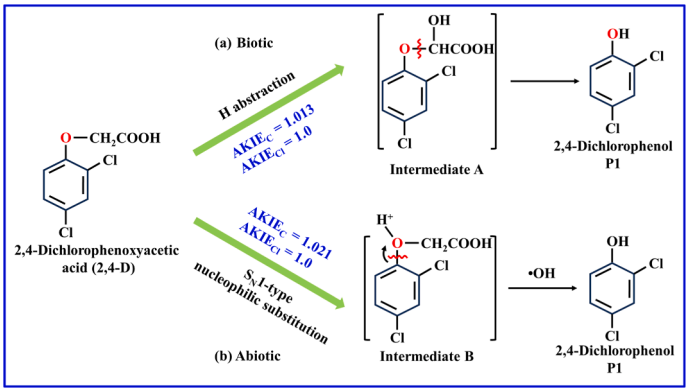


## ARTICLE INFO

*Keywords:*
Multiple isotope fractionation
2,4-Dichlorophenoxyacetic acid
Biodegradation,simulated sunlight irradiation
$Fe^{2+}/H_2O_2$, mechanism

## ABSTRACT

In this research, 2,4-dichlorophenoxyacetic acid was employed as a typical phenoxy acid herbicide to investigate carbon, hydrogen, and chlorine isotope fractionations, characterizing the underlying biotic and abiotic reaction mechanisms for the first time. For the biotic transformation involving an indigenous strain *Stenotrophomonas maltophilia* sp., a primary carbon and hydrogen isotope fractionations ($\varepsilon_C = -1.6 \pm 0.2$ ‰, $\varepsilon_H = -130.6 \pm 7.9$ ‰), and no chlorine isotope fractionation were observed. The calculated carbon and hydrogen apparent kinetic isotope effects ($AKIE_C = 1.013$, $AKIE_H = 4.621$) indicated that hydrogen abstraction from the methylene carbon of the side chain was the dominant rate-limiting step in the first reaction step. This was followed by the cleavage of the ether-oxygen bond, leading to the formation of the initial aromatic product 2,4-dichlorophenol. In contrast, for the abiotic transformation using $Fe^{2+}/H_2O_2$ under simulated sunlight

* Corresponding author at: Guangdong Key Laboratory of Environmental Catalysis and Health Risk Control, Guangdong-Hong Kong-Macao Joint Laboratory for Contaminants Exposure and Health, Institute of Environmental Health and Pollution Control, Guangdong University of Technology, Guangzhou 510006, China.
*E-mail address:* xjuk2017@gdut.edu.cn (J. Xiong).

https://doi.org/10.1016/j.jhazmat.2025.139885
Received 26 June 2025; Received in revised form 8 September 2025; Accepted 14 September 2025
Available online 15 September 2025

irradiation, a primary carbon isotope fractionation ($\varepsilon_C = -2.7 \pm 0.2$ ‰) was observed. The calculated $AKIE_C$ value of 1.021 indicated that the cleavage of the ether-oxygen bond between the aromatic carbon and the ether oxygen was the dominant rate-limiting step, consistent with an $S_N1$-type nucleophilic substitution. Therefore, multiple isotope fractionations may serve as a valuable tool for identifying significant transformation pathways contaminated groundwater sites.

## 1. Introduction

Phenoxyalkanoic acids are a class of herbicides that have been extensively used in both agricultural fields and non-cropland areas to control the growth of broadleaf weeds since the mid-20th century. One of the most significant phenoxyalkanoic acid herbicides is 2,4-dichlorophenoxyacetic acid (2,4-D), which has been widely employed to control broadleaf weeds in crops such as wheat, corn, cotton, soybean, and tobacco, as well as in nonagricultural soils [1, 2]. Consequently, it is frequently detected in soils, surface waters, and groundwaters at concentrations ranging from several to hundreds of micrograms per liter [3, 4]. Although 2,4-D exhibits moderate persistence with relatively short half-lives in soils, it poses a potential risk as a contaminant in surface water and groundwater due to its relatively high water solubility and low sorption to soils [5]. Therefore, to protect natural ecosystems and human food resources, it is crucial to understand the fate and transformation pathways of 2,4-D in aquatic environments.

The transformation of 2,4-D involves both biotic and abiotic processes in environmental waters [6, 7]. The biotic transformation has been extensively studied in microbial, plant, and animal systems. Since the mid-20th century, numerous strains of microorganisms capable of degrading 2,4-D have been isolated, and two major metabolic pathways have been identified. In bacteria such as *Pseudomonas*, *Arthrobacter*, and *Alcaligenes* sp., 2,4-D serves as the sole carbon source under aerobic conditions and is initially transformed by the cleavage of the ether-oxygen (C-O) bond. This process produces a major product 2, 4-dichlorophenol (2,4-DCP), through the loss of the alkanoic side chain [8, 9]. The white rot fungus, *Phanerochaete chrysosporium* can transform 2,4-D by cleaving the C-O bond in the initial step [10]. However, other studies suggest that reductive dehalogenation occurs at the chlorine atom in the 2-position, leading to the formation of 4-chlorophenoxyacetic acid through the cleavage of the C-Cl bond instead of the C-O bond in the first step [11–14]. These findings indicate that the biotic transformation of 2,4-D may involve two primary mechanisms, resulting in different products derived from the same initial compound in aqueous environments.

The widespread use of 2,4-D has prompted numerous studies on its photochemical transformation in aqueous environments. In groundwater, 2,4-D is resistant to hydrolysis [15, 16], while in surface waters, light-induced transformation represents a significant pathway for its degradation [6]. Two distinct mechanisms have generally been proposed for light-induced reactions: direct photo-transformation and indirect photo-transformation [17]. Arkhipova and colleagues [18] observed a rapid direct photo-transformation of 2,4-D in aqueous solution through UV irradiation and suggested that the primary pathways involve the homolysis of the C-O and C-Cl bonds, followed by a cascade of various free radical reactions. Crosby and Tutass [19] detected the products 2,4-DCP, 4-chlorocatechol, 2-hydroxy-4-chlorophenoxyacetic acid, and 1,2,4-benzenetriol during the direct photodecomposition of 2,4-D via UV irradiation. They proposed that the major reaction involves the cleavage of the C-O bond to produce 2,4-DCP, while the minor reaction involves dehalogenation through C-Cl bond cleavage, resulting in the formation of 2-hydroxy-4-chlorophenoxyacetic acid. However, ultraviolet radiation from sunlight is not expected to decompose 2,4-D [16]. In surface waters, 2,4-D can undergo indirect photo-transformation through reactive oxygen species [13] such as hydroxyl radicals ($^{\bullet}OH$), which can be generated by the irradiation of photosensitizers (e.g., dissolved natural organic matter) [6, 20]. Advanced oxidation processes for the treatment of contaminated water and wastewater operate on the same principle [21, 22]. Reactions such as the degradation of alkyl substituent moieties, hydroxylation of unsubstituted aryl positions, and aryl substitution reactions all occur concurrently during the transformation and are typically attributed to $^{\bullet}OH$ [23]. In $^{\bullet}OH$-induced oxidative transformation, the most prevalent intermediate in the reaction between $^{\bullet}OH$ and 2,4-D is 2,4-DCP [21, 22]. The $^{\bullet}OH$ attacks at carbon of the aromatic ring, followed by the loss of an alkoxy radical or anion, resulting in the formation of 2,4-DCP. Alternatively, hydrogen abstraction from the methylene carbon of the side chain, followed by the trapping of the resulting $^{\bullet}OH$ and the cleavage of the C-O bond, also produces 2,4-DCP. The two pathways differ in the mechanism of C-O bond cleavage. Therefore, studying the competition between $^{\bullet}OH$ addition to the aromatic ring and side chain attack is essential for predicting the behavior of 2,4-D in field environments.

Generally, transformation pathways can be investigated by monitoring contaminant concentrations and identifying daughter products. However, changes in concentration within contaminated fields can be influenced by various physical processes, which may not provide sufficient information to elucidate transformation pathways. The mere presence of products does not always yield clear insights for identifying transformation pathways, as different pathways can produce the same products [24, 25]. Compound-specific isotope analysis (CSIA) has emerged as an innovative tool for characterizing specific transformation pathways, as it reflects the magnitude of isotope fractionations at different reactive sites [26]. Isotope fractionation can be traced back to underlying kinetic isotope effects (KIE), which characterizes the rate-limiting step relevant to a given reaction mechanism, potentially involving the cleavage or formation of chemical bonds. However, interpreting experimental data based on the isotope fractionation of a single element can introduce bias in the characterization of transformation pathways. Hence, evidence of dual or multi-dimensional elements is essential for distinguishing between different transformation pathways. Influences such as masking, which arise from the rate-limiting steps preceding bond cleavage, would affect both elements equally. This approach has been employed, for example, to differentiate between the acid-catalyzed hydrolysis pathway involving the *tert*-butyl group (an $S_N1$ reaction) and the hydrolysis pathway by nucleophilic attack at the methyl group ($S_N2$ reaction) for methyl tert-butyl ether (MTBE) [24, 27]. It has also been used to distinguish between the stepwise dichloroelimination pathway and the concerted dichloroelimination pathway for 1,1,2-trichloroethane [28], as well as between the aromatic ring addition pathway and the side chain oxidation pathway for various substituted aromatic compounds [29]. In the case of phenoxyalkanoic acid herbicides in aqueous environments, no associated C, H, and Cl isotope fractionation has been reported in previous studies.

Therefore, we conducted a systematic investigation of the biotic and abiotic transformations of 2,4-D using an aerobic indigenous strain *Stenotrophomonas maltophilia* sp., in conjunction with an $Fe^{2+}/H_2O_2$ system and simulated sunlight irradiation. This study aimed to explore the oxidation pathways of the aromatic ring and its substituents through multi-dimensional isotope analysis. We determined the C and H isotope enrichment factors ($\varepsilon_C$ and $\varepsilon_H$) for the cleavage of the C-O bond ($C_1$-O or $C_1$'-O) to examine the resonance and inductive effects of different pathways on isotope fractionation. The mechanisms of the reaction pathways, in which substituents were lost (either through attack on the aromatic ring or cleavage of the side chain) were identified based on the

observed isotope fractionation and the reaction products. Consequently, multi-dimensional isotope analysis could pave the way for characterizing the biotic and abiotic transformation pathways of 2,4-D and other phenoxyalkanoic acid herbicides.

## 2. Materials and methods

### 2.1. Chemicals

2,4-Dichlorophenoxyacetic acid (2,4-D, CAS: 94–75–7, ≥ 98.0 %) was purchased from ANPEL Laboratory Technologies (Shanghai) Inc., China. Boron trifluoride – methanol solution ($BF_3$•MeOH, CAS: 373–57–9, 10 % in methanol, w/v) was obtained from Shanghai Macklin Biochemical Co., Ltd. 2,2,6,6-Tetramethylpiperidine (TMPD, CAS: 768–66–1, ≥ 99.0 %) and 5,5-dimethyl-1-pyrroline N-oxide (DMPO, CAS: 3317–61–1, ≥ 97.0 %), which were used to trap the ROSs were sourced from Aldrich and J&K, respectively. GC-grade methanol (MeOH) was purchased from Merck (Germany), while GC-grade *n*-hexane and ethyl acetate were obtained from CNW (ANPEL). Other reagents were of at least reagent grade and were supplied by Guangzhou Chemical Reagent Factory, China. A 1000 mg/L concentration of the 2,4-D stock solution was prepared by dissolving the appropriate amount of 2,4-D in MeOH. The compositions of the growth medium (GM) and mineral salt medium (MSM) used for biodegradation were based on our previous study [30]. The pH of the MSM was adjusted to 7.0 for the experiments and autoclaved at 121 °C for 30 min.

### 2.2. Biodegradation of 2,4-D

The bacterial strain was cultured in Luria-Bertani (LB) medium for 24 h with continuous shaking at 160 rpm under dark conditions. Following this, biodegradation experiments were conducted to assess the strain's performance under various conditions. Detailed methods for the isolation and identification of the indigenous strain are provided in the Supporting Information (SI) (Section S1). Unless otherwise specified, biodegradation experiments involved inoculating 0.2 g of the exponentially growing bacterial strain into 100 mL of MSM containing 0.1 mg of 2,4-D in 250 mL Erlenmeyer flasks, which were maintained under dark conditions at 37 °C, pH 7.0, and 160 rpm. To simulate environmental concentrations of 2,4-D, 0.05, 0.1, 0.5, 2.5, and 5.0 mg of 2,4-D were utilized in the experiments. For each batch of experiments, one parameter was varied while the others were remained constant. All samples were analyzed in triplicate.

For the degradation of 2,4-D by crude enzymes derived from the bacterial strain, the bacterial culture was first separated from LB broth by centrifugation at 8000 rpm for 2 min. The supernatant was collected as the extracellular crude enzyme. Subsequently, the separated bacteria were washed and resuspended in sterile phosphate-buffered saline (PBS) for further treatment. The bacterial suspension was subjected to sonication for 10 min in an ice water bath, with 2 s intervals between each burst. After centrifugation at 8000 rpm for 10 min to remove bacterial debris, the resulting supernatant was filtered through a 0.22 $\mu$m pore size filter, and the filtrate was designated as the intracellular crude enzyme. The degradation of 2,4-D using both extracellular and intracellular crude enzymes was conducted in 50 mL Erlenmeyer flasks containing 1.0 mg/L of 2,4-D in the dark. The pH was adjusted to 7.0, and residual 2,4-D was measured at 0, 24, 48, 72, 96, 120, and 144 h, respectively. The treatment without crude enzyme served as the control.

### 2.3. Photochemical degradation of 2,4-D

To compare the biotic with abiotic transformation of 2,4-D by using multi-dimensional isotope fractionation, the photochemical degradation of 2,4-D was investigated. According to previous studies [6, 17, 23, 31, 32], the $Fe^{2+}/H_2O_2$ system under simulated sunlight irradiation was chosen in experiments. The photochemical reaction was conducted in a Pyrex reactor using a 220 W xenon lamp as a simulated sunlight source, emitting a broad continuous spectrum ranging from 180 to 1200 nm. A filter with a 280 nm cut-off wavelength was applied, as wavelengths equal to or greater than 280 nm are typical at the Earth's surface. The xenon lamp was activated on for a period until the light sources stabilized. Quartz tube reactors were utilized throughout these experiments, with eight channels operating simultaneously. A solution of 5 mM of 2, 4-D in 50 mL of sodium phosphate buffer (pH 4.0) was placed in the reactor, to which $Fe^{2+}/H_2O_2$ was added, resulting in an initial molar ratio of 6.5:1 for $Fe^{2+}/H_2O_2$ to 2,4-D. The pH = 4.0 was used to increase the solubility and inhibit hydrolysis of 2,4-D. While the concentration of $Fe^{2+}$ and $H_2O_2$ were selected according to Fenton's reagent. The solution was continuously mixed on a magnetic stirrer at 300 rpm during the experiment and maintained at a temperature of (25 ± 1) °C. Aliquots were taken at various intervals through a rubber septum of the reactor using a syringe and filtered with a 0.22 μm polycarbonate filter membrane. A volume of 1.0 mL of methanol was added to terminate the reaction. Control experiments were conducted with xenon lamp irradiation alone, and $H_2O_2$ alone. All samples were prepared in triplicate and stored at 4 °C until analysis.

### 2.4. Instrumentation analysis

*HPLC analysis*: The concentrations of 2,4-D were determined using a high-performance liquid chromatography (HPLC) (Agilent 1260, USA) equipped with a UV detector set to 235 nm. Separation was achieved on a C-18 column (4.6 mm i.d. × 150 mm, 5 μm). The column temperature was maintained at 35 °C. The eluent consisted of a mixed solution of 80 % MeOH (mobile phase A) and 20 % ultra-pure water (mobile phase B, containing 0.2 % formic acid) at a flow rate of 1.0 mL/min. The sample injection volume was 20 $\mu$L.

*EPR analysis*: Electron paramagnetic resonance (EPR) spectra were recorded using a Bruker EMX Plus-10/12 spectrometer (Bremen, Germany), operated at 20 mW microwave power (9.85 GHz) with sweep width of 100 G and modulation frequency of 100 kHz. The center field was set to 3510 G. A 50 μL sample was placed in a quartz flat cell with a total capacity of 50 μL and irradiated directly inside the microwave cavity of the spectrometer using a 1 kW Xe arc lamp. Radiation from the lamp passed through a 30 mm pathlength liquid filter (λ > 400 nm; aqueous solution containing in g/L: $NaNO_2$ 48.4, $Na_2CO_3$ 1.0, and $K_2CrO_4$ 0.2) to eliminate wavelengths below 400 nm. Hyperfine coupling constants were obtained by accumulating, simulating, and optimizing spectra on an IBM PC computer using software described in previous studies [33]. The accuracy of the coupling constant measurement was ± 0.02 G. Fremy's salt was used as a standard for determining of the EPR spectral g-value. TMPD served as the spin trap for singlet oxygen ($^1O_2$), while DMPO was employed to trap singlet superoxide ($O_2^{\bullet-}$) and $^{\bullet}OH$ [32]. The time between the initiation of the reaction and the onset of EPR scanning was controlled to be less than 80 s.

*GC-MS analysis*: The derivative of 2,4-D (Section S2) and its degradation products were identified using an Agilent 5977 mass spectrometer coupled with an Agilent 7890B gas chromatograph (GC-MS). The chromatographic column employed was an HP-5 MS (30 m × 0.25 mm × 0.25 $\mu$m, 19091S-433; temperature limits: −60–325/350 °C, Agilent Technologies). Helium (99.999 %) served as the carrier gas at a flow rate of 1.0 mL/min. The oven temperature was initially held at 120 °C for 1 min, then programmed to increase to 180 °C at a rate of 10 °C/min, and subsequently ramped up to 280 °C at a rate of 20 °C/min, where it was held for an additional minute. The injection port and the interface were maintained at 280 °C. Samples of 1.0 μL were introduced in splitless mode. Mass spectra were obtained in electron ionization (EI) mode at an ion source temperature of 230 °C and an electron energy of 70 eV.

*GC-C/Py-IRMS analysis*: The carbon stable isotope compositions ($\delta^{13}C$) of 2,4-D were measured using a gas chromatography – combustion – isotope ratio mass spectrometer (GC-C-IRMS) [32], following

previously described methods with modifications. A sample of 2.0 μL was injected with a split ratio of 10:1 into a split injector at 290 °C with a flow rate of 1.1 mL/min. Helium (99.999 %) was used as the carrier gas. The analytical column employed was an HP-5 MS (30 m × 0.32 mm × 0.25 μm, 19091S-413, temperature limits: −60–325/350 °C, Agilent Technologies). The GC oven was programmed to start at 120 °C (held for 1 min), then ramped at a rate of 10 °C/min to 180 °C, followed by a ramp of 20 °C/min to 280 °C (held for 1 min). Carbon dioxide ($\delta^{13}C$ = −21.66 ‰) was introduced as a reference gas into the IRMS automatically at the beginning and end of each sample to calibrate the instrument's stability. All samples were analyzed in triplicate, with standard deviations of ≤ ±0.5 ‰ (1σ) for carbon.

Changes in hydrogen isotope ratios ($\delta^{2}H$) were determined using a gas chromatography – high-temperature pyrolysis – isotope ratio mass spectrometry (GC-Py-IRMS) [34, 35]. The system comprised of a GC (6890 series, Agilent Technologies) coupled with a high-temperature conversion interface (GC-TC, ThermoFinnigan, Bremen, Germany), which was connected to a Trace 1300–253 plus IRMS. The ceramic reactor tube was packed with chromium and used as the TC reactor at 1350 °C. The use of chromium and chemical sequestration of Cl by chromium result in quantitative conversion of compound-specific organic hydrogen to $H_2$ analyte gas. A sample of 2.0 μL was injected with a splitless into the injector at 290 °C with a flow rate of 1.1 mL/min. Helium (99.999 %) was used as the carrier gas. The analytical column employed was an HP-5 MS (30 m × 0.32 mm × 0.25 μm, 19091S-413, temperature limits: −60–325/350 °C, Agilent Technologies). The GC oven was programmed to start at 120 °C (held for 1 min), then ramped at a rate of 10 °C/min to 180 °C, followed by a ramp of 20 °C/min to 280 °C (held for 1 min). All samples were analyzed in triplicate, with standard deviations of ≤ ±2 ‰ (1σ) for hydrogen.

*GC-qMS analysis:* The stable isotope compositions of chlorine ($\delta^{37}Cl$) in 2,4-D were analyzed using an Agilent 7890B gas chromatograph connected to an Agilent 5977B quadrupole mass spectrometer (GC-qMS) operating in electron impact (EI) mode with selective ion monitoring. The system was equipped with an HP-5 MS column (30 m × 0.25 mm × 0.25 μm, 19091S-433; temperature limits: −60–325/350 °C, Agilent Technologies). Helium (99.999 %) served as the carrier gas at a flow rate of 1.0 mL/min. The oven temperature was initially held at 120 °C for 1 min, then programmed to increase to 180 °C at a rate of 10 °C/min, and subsequently ramped to 280 °C at a rate of 20 °C/min, where it was held for an additional minute. The injection port and interface were maintained at 280 °C. A sample volume of 1.0 μL was introduced in splitless mode. Mass spectra were obtained in EI mode with an ion source temperature of 230 °C and an electron energy of 70 eV. The chlorine isotope ratios ($^{37}Cl/^{35}Cl$) were calculated as previously reported in the literature [36].

Carbon, hydrogen, and chlorine isotope compositions were reported as $\delta^{13}C$, $\delta^{2}H$, and $\delta^{37}Cl$ in per mil (‰) relative to Vienna PeeDee Belemnite (VPDB), Vienna Standard Mean Ocean Water (VSMOW), and Standard Mean Ocean Chloride (SMOC), respectively [37, 38]. The isotope fractionation during the reaction was calculated using the Rayleigh equation (Eq. 1):

$$\ln\frac{\delta_t + 1000}{\delta_0 + 1000} = \varepsilon \times \ln f \tag{1}$$

Where $\delta_t$ and $\delta_0$ represent the isotope ratios of the substrate at times $t$ and 0 ($t = 0$ is the start time of the experiment, and $t = t$ is any time of the experiment), respectively, and $f$ denotes the remaining fraction of substrate at time $t$, defined as the ratio of substrate concentration at time $t$ to the initial concentration ($f = C_t/C_0$). The obtained slope, $\varepsilon$, corresponds to the bulk isotopic enrichment factor.

Apparent kinetic isotope effects (AKIEs) for reactive positions were calculated using Eq. 2 [39, 40].

$$\text{AKIEs} = \frac{1}{1 + \frac{n}{x} z\, \varepsilon \Big/ 1000} \tag{2}$$

Where $\varepsilon$ represents the obtained bulk isotope enrichment factor, $n$ denotes the number of atoms of the element under consideration in the molecule, $x$ indicates the number of reactive positions, and $z$ signifies the number of indistinguishable reactive sites.

For analyzing the methylated 2,4-D, two ions of the molecular group ($m/z$ 236 and 238) were measured with GC-qMS instrument. For the methylated 2,4-D, the intensities of the most abundant fragment ion peaks are much higher than those of the parent ion peaks. Ion couple ($m/z$ 236 and 238) correspond to isotopologue pair ($[^{37}Cl_2^{12}C_9^{16}O_3^1H_8]^+$ and $[^{37}Cl^{35}Cl^{12}C_9^{16}O_3^1H_8]^+$, respectively) that differ by one heavy chlorine isotope. The isotope ratio (R) can be obtained from the ratio of these isotopologues according to Eq. 3 [41–43]:

$$R(^{37}Cl/^{35}Cl) = \frac{^{37}Cl}{^{35}Cl} = \frac{^{37}p}{^{35}p} = \frac{k}{n-k+1} \times \frac{^{37}1_{(k)}C^{35}Cl_{(n-k)}}{^{37}1_{(k-1)}C^{35}Cl_{(n-k+1)}} = 2 \times \frac{^{238}I}{^{236}I} \tag{3}$$

Where $^{37}p$ and $^{35}p$ are the probabilities of encountering $^{37}Cl$ and $^{35}Cl$, respectively, $n$ is the number of Cl atoms, $k$ is the number of $^{37}Cl$ isotopes, $^{37}Cl_{(k)}^{35}Cl_{(n-k)}$ and $^{37}Cl_{(k\text{-}1)}^{35}Cl_{(n\text{-}k+1)}$ represent the isotopologues containing $k$ and $k$-1 heavy isotopes, respectively, and I indicate the peak intensity of each ion. The $\delta^{37}Cl$ values were determined by referencing versus an external methylated 2,4-D working standard according to Eq. 4 [44]:

$$\delta Cl^{37}_{\text{sample}} = \frac{R(Cl_{37}/Cl_{35})_{\text{sample}}}{R(Cl_{37}/Cl_{35})_{\text{standard}}} - 1 \tag{4}$$

## 3. Results and discussion

### 3.1. Biodegradation of 2,4-D

The biodegradation of 2,4-D by *Stenotrophomonas maltophilia* sp., which was isolated from farmland soil, was investigated in this study. The morphological, physiological, and biochemical characteristics of the strain are presented in Tab. S1, Fig. S1, and Fig S2. The effects of various key parameters, including initial concentrations, temperature, pH values, and inoculum volumes, on the biodegradation of 2,4-D were examined at a fixed shaking speed of 160 rpm. The results indicated that the biodegradation efficiencies of 2,4-D were influenced by its initial concentrations (Fig. 1a). The biodegradation efficiencies were 82.5 %, 80.5 %, 72.5 %, 66.4 %, and 51.9 % for initial concentrations of 0.5, 1, 5, 25, and 50 mg/L, respectively. The corresponding half-lives were 54, 59, 71, 85, and 126 h, respectively. As concentrations increased, the biodegradation efficiencies decreased, which may be due to the saturation of 2,4-D for bacteria degradation and/or the toxicity effects of 2,4-D to *Stenotrophomonas maltophilia* sp. by inhibiting the activities of the related degrading enzymes [13].

Temperature is a critical factor in the biodegradation of pollutants [45]. The effects of temperature on the biodegradation of 2,4-D are illustrated in Fig. 1b. The results indicate that biodegradation efficiency increased as the temperature rose from 20 to 35 °C, reaching a maximum efficiency of 76.9 % at 35 °C. However, as the temperature continued to rise to 40 °C, biodegradation efficiency gradually decreased to 49.0 %. Therefore, the optimum temperature for 2,4-D biodegradation is 35 °C. In a previous study, the optimal temperature for the biodegradation of deltamethrin by *Stenotrophomonas maltophilia* XQ08 was also determined to be 35 °C [46].

The optimal pH value and inoculum volume for the biodegradation of 2,4-D were determined to be 7.0 and 1.0 g/L, respectively (Figs. 1c and 1d). When the pH varied from 4.0 to 9.0, the biodegradation efficiencies ranged from 10.9 % to 76.7 %, with the maximum efficiency occurring at pH 7.0. Neutral pH values were more favorable for 2,4-D

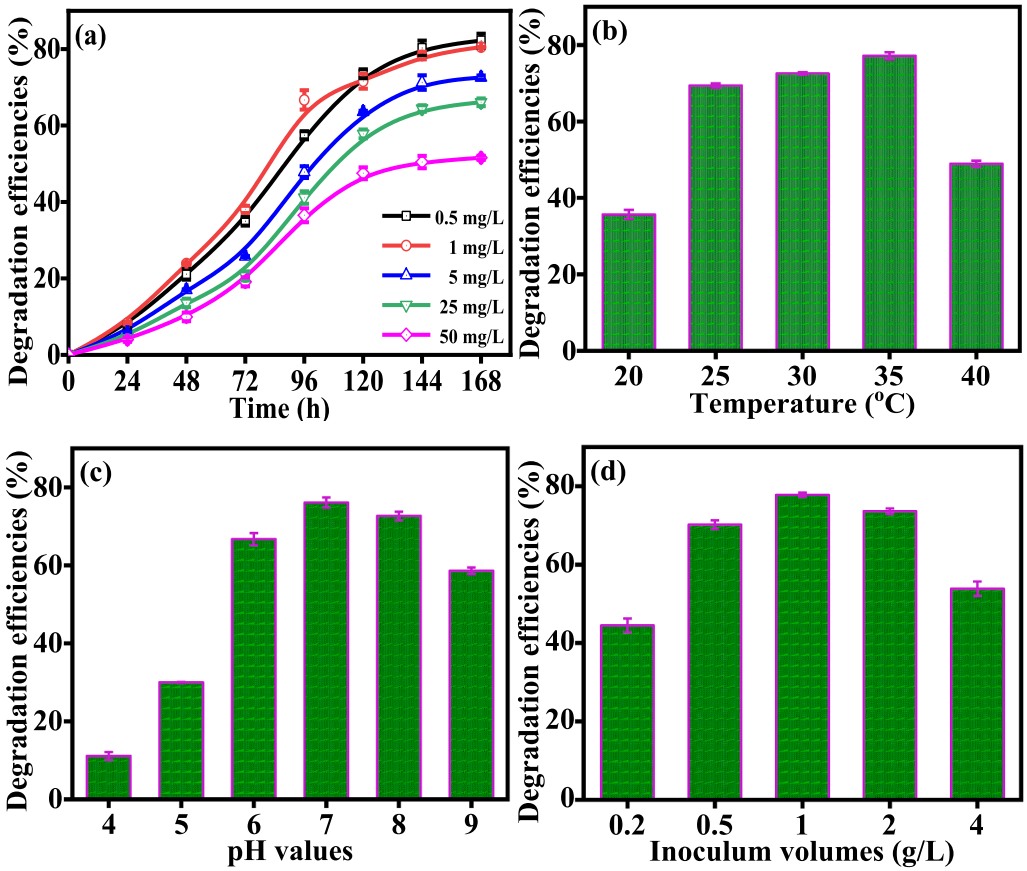


**Fig. 1.** The effects on 2,4-D biodegradation. (a) 2,4-D concentrations (mg/L): 0.5 (□); 1 (○); 5 (△); 25 (▽); 50 (◇); (b) temperatures; (c) pH values; (d) inoculum volumes (error bars represented standard deviations).

biodegradation. These results can be attributed to the stability and activity of enzymes secreted by *Stenotrophomonas maltophilia* sp. under varying pH conditions. Additionally, the findings indicated that biodegradation efficiencies were influenced by inoculum volume (Fig. 1d). The efficiencies increased steadily from 44.5 % to 77.8 % as the inoculum volume rose from 0.2 to 1.0 g/L, achieving a maximum degradation efficiency of 77.8 % at an inoculum volume of 1.0 g/L. However, biodegradation efficiencies gradually declined with further increases in inoculum volume. This decrease may be due to high bacterial concentrations inhibiting respiration and degradation activity. A previous study also reported that the biodegradation efficiencies of chloramphenicol by *Aeromonas media* SZW3 were affected by the initial bacterial dosage [47].

### 3.2. Degradation of 2,4-D by bacteria, extracellular and intracellular enzymes

The degradation of organic contaminants by bacteria primarily occurs through enzymatic reactions involving the contaminants and various enzymes synthesized and secreted by the bacteria. Tang *et al.* [48] investigate the degradation of 2,2′,4,4′-tetrabrominated diphenyl ether (BDE-47) by *Pseudomonas aeruginosa* YH and find that the functional degradation enzymes are predominantly located within the cells, with the degradation of BDE-47 facilitated by intracellular enzymes. In contrast, Cao *et al.* [49] report that the functional degradation enzymes of responsible for BDE-47 degradation by *Phanerochaete* are mainly found outside the cells, with degradation occurring through the action of extracellular enzymes, while intracellular enzymes show no significant degradation effect. These studies, along with numerous related investigations, underscore the importance of determining whether the transformation of contaminants occurs via extracellular or intracellular enzymes, as this distinction is crucial for understanding the mechanisms of contaminant transformation.

In this study, we compared the degradation of 2,4-D by bacteria, extracellular crude enzymes, and intracellular crude enzymes (Fig. 2). The results indicated that the degradation rates of 2,4-D by bacteria and intracellular enzymes gradually increased over time, remaining similar until 72 h, after which the degradation rates stabilized at 168 h. In contrast, the degradation rates of 2,4-D by extracellular enzymes were

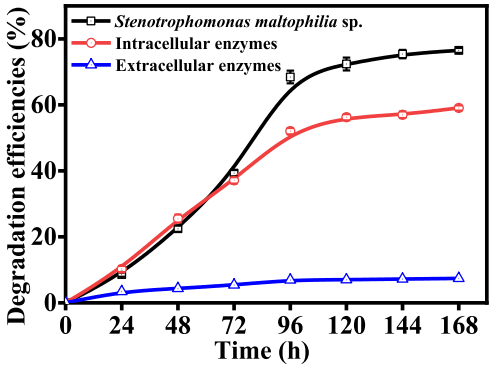


**Fig. 2.** Degradation of 2,4-D using the *Stenotrophomonas maltophilia* sp., intracellular and extracellular enzymes (error bars represented standard deviations).

lower than those of bacteria and intracellular enzymes and could be ignored considered negligible. This may be attributed to the fact that the functional degradation enzymes responsible for 2,4-D degradation are located within the cells, allowing for direct contact with 2,4-D and facilitating enzymatic reactions. Consequently, the degradation process is influenced by absorption and transmembrane transport. After 72 h, the degradation rates of 2,4-D by bacteria surpassed those of intracellular enzymes, while the degradation rates by extracellular enzymes remained negligible. This phenomenon may be explained by the induction of transcription and translation of certain oxidase and reductase genes by 2,4-D during the bacterial degradation process, leading to the secretion of more specific functional enzymes and resulting in enhanced degradation efficacy. Furthermore, the activity of intracellular enzymes decreased following interaction with 2,4-D, although bacteria may possess various mechanisms to repair functional enzymes. Previous studies have indicated that the biodegradation of 2,4-D by *Cupriavidus gilardii* T-1 involves several functional enzymes, including dioxygenase, hydroxylase, and cytochrome P450 [50, 51]. The minimal decrease in 2, 4-D within the extracellular enzyme system may be attributed to the absorption of 2,4-D by these enzymes. These findings are consistent with the degradation of tricresyl phosphate isomers by a novel microbial consortium [52].

### 3.3. Photochemical degradation of 2,4-D

The photochemical reaction is one of the most significant transformation processes of 2,4-D in surface aqueous environments [6]. Therefore, the photochemical transformation of 2,4-D using $Fe^{2+}/H_2O_2$ under simulated sunlight irradiation was investigated. The results indicated that 2,4-D undergoes efficient degradation when subjected to the oxidation process of $Fe^{2+}/H_2O_2$ under simulated sunlight, achieving a conversion efficiency of 84.9 % within 60 min. In contrast, relatively slow conversion efficiencies (less than 10 %) were observed when using $H_2O_2$ alone or simulated sunlight irradiation alone for the same duration (Fig. 3a). Previous studies have reported that the $Fe^{2+}/H_2O_2$-mediated photochemical transformation of organic compounds is primarily attributed to the reaction of $^{\bullet}OH$ with the organic compounds [22, 53].

To confirm that $^{\bullet}OH$ was the primary oxidizing species, we conducted ROSs scavenging experiments and EPR measurements. When methanol or tert-butanol was introduced into the $Fe^{2+}/H_2O_2$ system under simulated sunlight irradiation as a physical trap for $^{\bullet}OH$, the photochemical degradation was nearly completely inhibited (Fig. 3b). This indicates that the photochemical degradation of 2,4-D primarily involved a chemical reaction with $^{\bullet}OH$.

The presence of $^{\bullet}OH$ involved in the photochemical transformation of 2,4-D was confirmed through EPR analysis. DMPO was utilized as a probe for detecting $^{\bullet}OH$. The EPR spectra of the aqueous solution exhibited the characteristic four-line signal of the DMPO-$^{\bullet}OH$ spin adduct at various reaction time points (Fig. 4a). These results further confirmed that $^{\bullet}OH$ was generated in the $Fe^{2+}/H_2O_2$ system under simulated sunlight irradiation. Additionally, TEMP was employed as a probe for $^1O_2$. However, the EPR spectra of the aqueous solution did not display the characteristic three peaks of the TEMP-$^1O_2$ spin adduct (Fig. 4b), indicating that $^1O_2$ was not generated during the reaction.

### 3.4. Products identification

The transformation products of 2,4-D by *Stenotrophomonas maltophilia* sp. and through photochemical reactions were identified using a comparative procedure that included molecular weight analysis, isotopic distribution, and MS fragment analysis based on GC-MS. Some products were not identified due to their low concentrations in the reaction mixtures. Two metabolites, 2,4-DCP and 3,5-dichlorocatechol, were identified during biodegradation (Scheme 1). The mass spectra of these two metabolites indicated that they could be characterized by isotopic peaks at $m/z$ 162.00 and 178.99, respectively (Fig. S3). The chemical structures and retention times of the metabolites are summarized in Tab. S2. For the photochemical transformation of 2,4-D, five primary products were identifed: 2,4-DCP, 4,6-dichlororesorcinol, 4-chlorophenol, 2-chlorohydroquinone, and phenol (Scheme 1). The mass spectra of these five intermediates revealed that they could be characterized by isotopic peaks at $m/z$ 162.00, 177.03, 128.01, 142.90, and 94.10, respectively (Fig. S4). The chemical structures and retention times of the intermediates are summarized in Tab. S3.

### 3.5. Isotope fractionation

To gain a deeper understanding of the underlying transformation mechanisms of 2,4-D, analyses of carbon, hydrogen, and chlorine isotopes were conducted during the processes of 2,4-D biodegradation and photochemical degradation. The Rayleigh equation was utilized to establish the relationship between changes in isotope composition and the degradation mechanisms.

*Carbon isotope fractionation*: During the biodegradation process conducted by *Stenotrophomonas maltophilia* sp., the carbon isotope ratio shifted from $-31.9 \pm 0.5$ ‰ to $-29.6 \pm 0.5$ ‰, corresponding to a degradation rate of 73.6 ‰. A carbon isotope effect ($\varepsilon_C = -1.6 \pm 0.2$ ‰), calculated using Eq. 1, was obtained (Figs. 5a and 5b). However, no carbon isotope fractionation was observed in the sterilized control (Fig. S5), confirming that only biodegradation was responsible for the changes in carbon isotope composition ($\delta^{13}C$) during the experiment. To gain a deeper understanding of the underlying mechanisms, the carbon apparent kinetic isotope effects ($AKIE_C$) were calculated to quantitatively characterize the isotope effects associated with chemical bond cleavage at the reactive position, as described in Eq. 2. This calculation considered the dilution effects of non-reactive positions

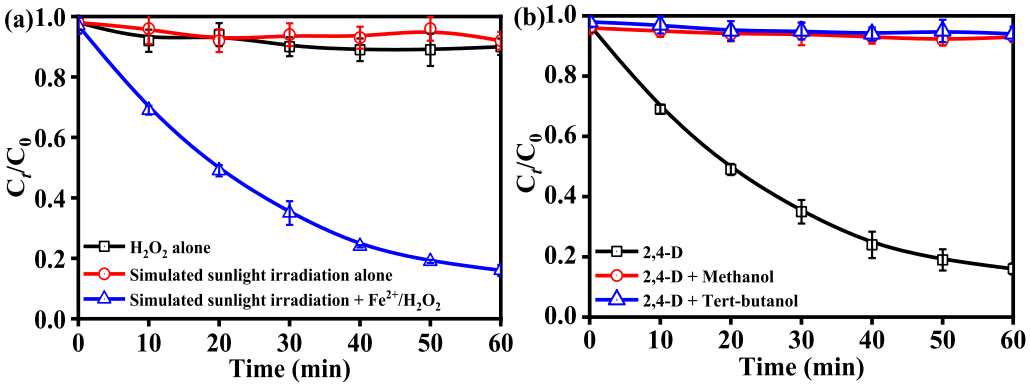


**Fig. 3.** Photochemical degradation of 2,4-D: (a) under $H_2O_2$ alone, simulated sunlight irradiation alone, and $Fe^{2+}/H_2O_2$ under simulated sunlight irradiation; (b) $Fe^{2+}/H_2O_2$ systems with adding methanol or tert-butanol quencher under simulated sunlight irradiation (error bars represented standard deviations).

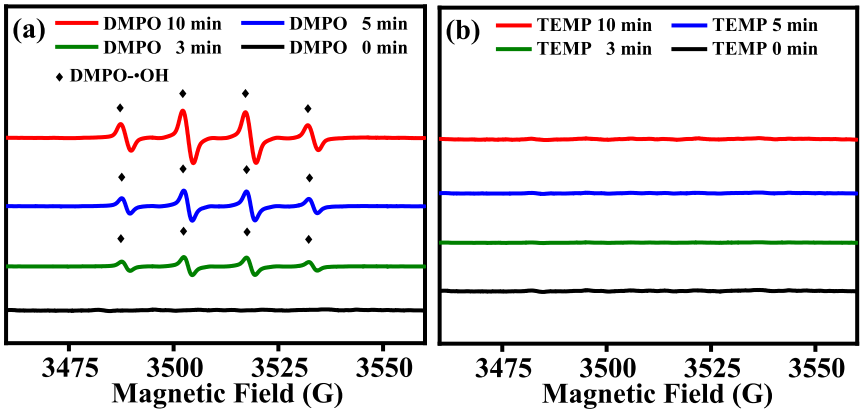


**Fig. 4.** EPR spectra of aqueous solution for $Fe^{2+}/H_2O_2$ under simulated sunlight irradiation. (a) $Fe^{2+}/H_2O_2$ under simulated sunlight irradiation and DMPO for different time points (0, 3, 5, 10 min); (b) $Fe^{2+}/H_2O_2$ under simulated sunlight irradiation and TEMP for different time points (0, 3, 5, 10 min).

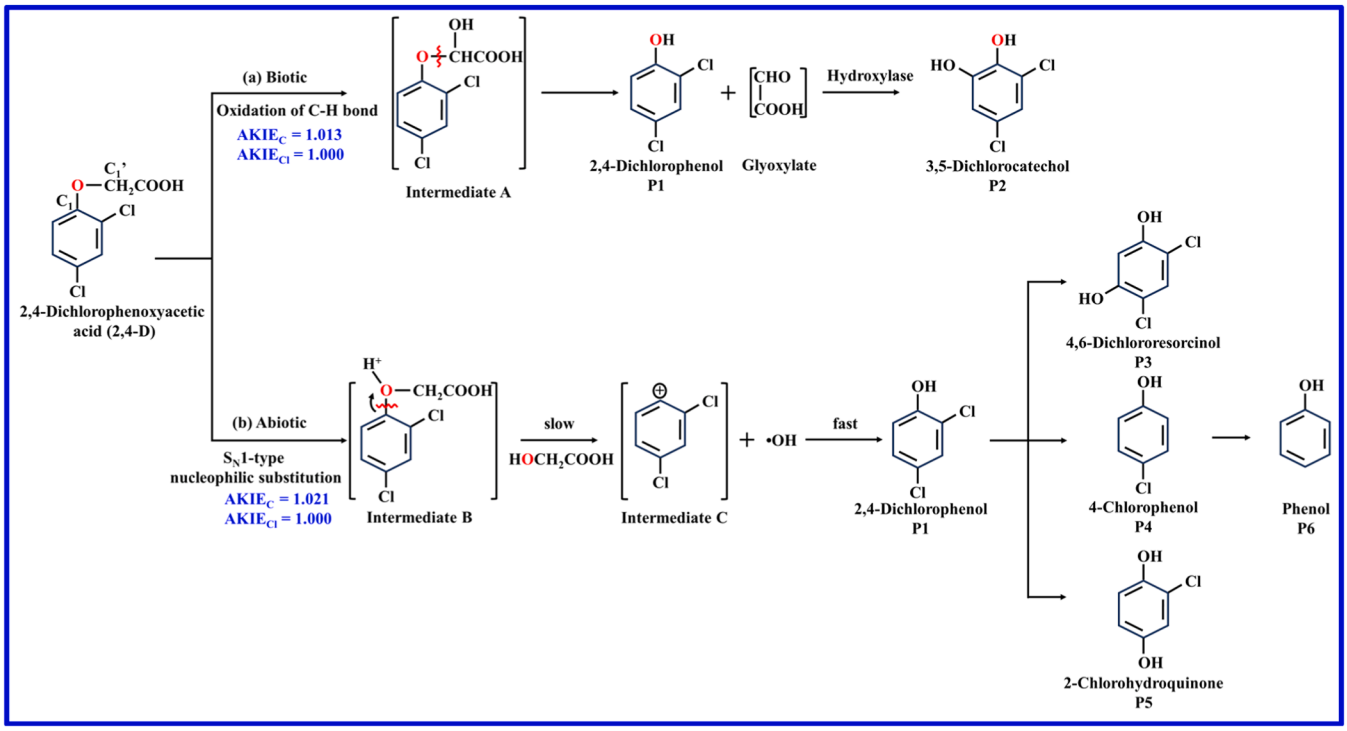


**Scheme 1.** Proposed 2,4-D biotic and abiotic transformation pathways.

within the molecules, as well as intramolecular competition. The $AKIE_C$ was determined under the assumption that all carbon atoms were chemically equivalent and that only carbon atoms participated in the reaction, which was assumed to occur via a stepwise process. Therefore, $n = 8$, and $x = z = 1$ were applied for the $AKIE_C$ calculation. The resulting $AKIE_C$ value was $1.013 \pm 0.0011$.

The $AKIE_C$ value of 1.013 falls within the typical range of carbon kinetic isotope effects ($KIE_C$) for the oxidative cleavage of C-H bonds [39], which is between 1.01 and 1.03. This indicates that the cleavage of a C-H bond is the primary rate-limiting step in the biodegradation process. Palau *et al.* [41] reported an approximate $AKIE_C$ of 1.007 during the aerobic biodegradation of 1,2-dichloroethane via oxidative cleavage of a C-H bond by *Pseudomonas* sp. strain DCA1. Similarly, Gray et al. [54] found an $AKIE_C$ range of 1.010–1.012 during the aerobic biodegradation of MTBE through C-H bond cleavage by a bacterial culture (PM1), which aligns with the $AKIE_C$ value measured in this study. However, the measured $AKIE_C$ value is relatively low compared to the typical $KIE_C$ and is somewhat smaller than the Streitwieser Semiclassical Limit for C-H bond cleavage, which is 1.021 [39]. This relatively low $AKIE_C$ value may be attributed to the masking of intrinsic isotope effects associated with C-H bond cleavage.

Recent reports have examined several biodegradation processes that may clarify the observed masking effects. Sherwood-Lollar et al. [55] noted smaller $AKIE_C$ values during the degradation of 1,1,1-trichloroethane by whole cells (1.004) and cell-free extracts (1.002), demonstrating significant masking of the measured $AKIE_C$ values compared to the intrinsic $KIE_C$ (1.030) observed in abiotic degradation experiments. The intrinsic $KIE_C$ can be substantially obscured in highly efficient enzymatic reactions, leading to predicted intrinsic $KIE_C$ values that are not realized [56]. Additionally, other rate-limiting factors (e.g., transport and binding to the enzymatic site, substrate activation in intermediate enzyme complexes, etc.) may also contribute to the reduction of intrinsic $KIE_C$ values. Nijenhuis et al. [57] reported significantly greater isotope fractionation for pure enzyme and cell free-extract experiments

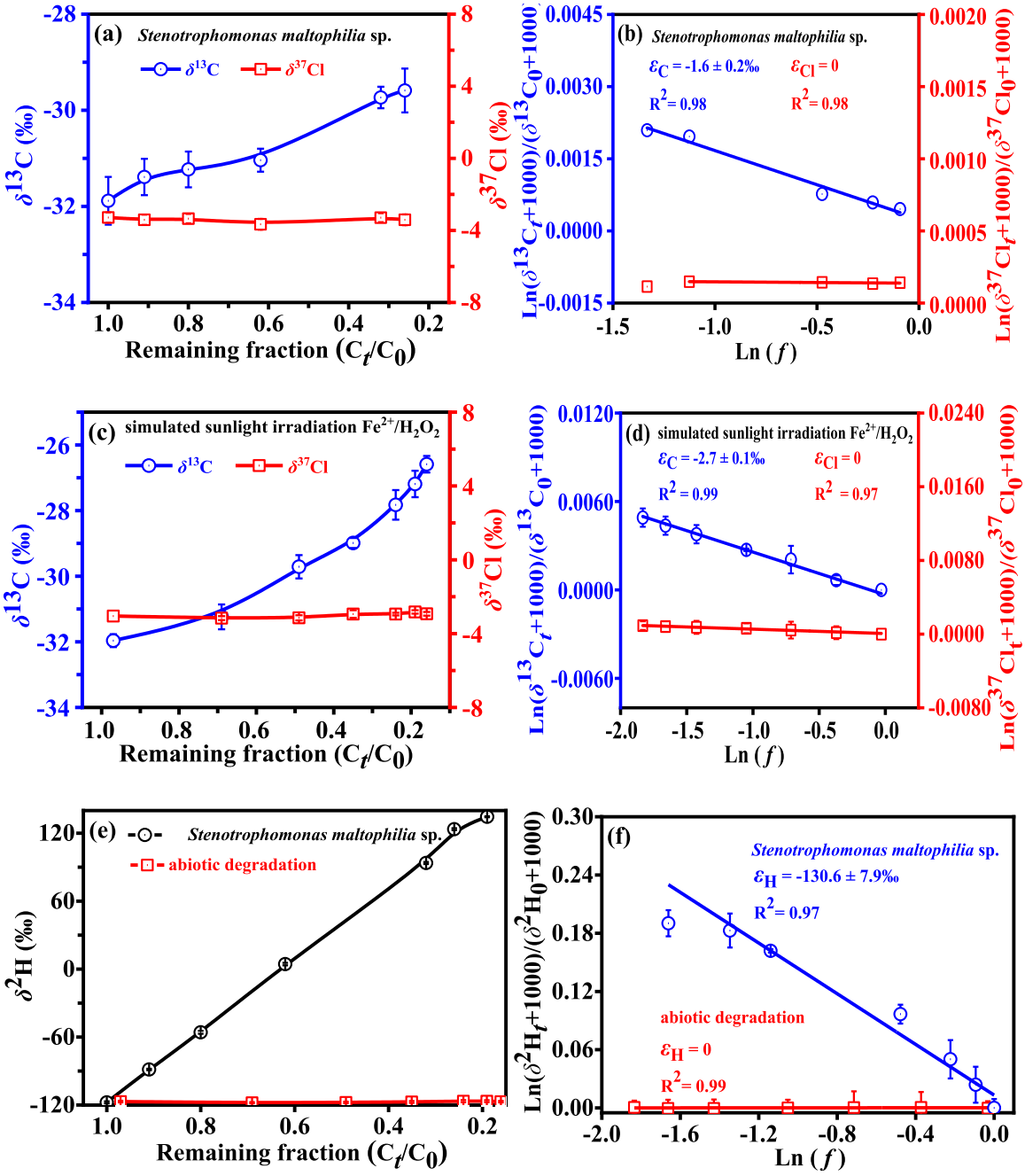


**Fig. 5.** Isotope fractionation of 2,4-D during degradation processes by *Stenotrophomonas maltophilia* sp. and $Fe^{2+}/H_2O_2$ under simulated sunlight irradiation. (a), (c), and (e) showed the evolution of $\delta^{13}C$, $\delta^{37}Cl$, and $\delta^{2}H$ values vs remaining fraction. (b), (d), and (f) showed the linearized isotope enrichment used to derive enrichment factors.

compared to whole cells during the anaerobic reductive dechlorination of tetrachloroethene, indicating that substrate transport across the cell membrane can considerably mask the intrinsic $KIE_C$. In this study, the observed lower $AKIE_C$ values during the degradation of 2,4-D by both whole cells (1.013) and cell-free extracts (1.012) (Fig. S6) were compared to the intrinsic $KIE_C$ (1.030) expected for the cleavage of a C-H bond. Since these values cannot be attributed to transport effects across the cell membrane, this suggests that the masking of the intrinsic $KIE_C$ occurs within the enzyme itself and is influenced by the enzyme's catalytic kinetics. Therefore, the $AKIE_C$ value (1.013) for 2,4-D biodegradation falls within the typical range $KIE_C$ (1.01–1.03) for the oxidative cleavage of a C-H bond, indicating that the cleavage of the C-H bond is the dominant rate-limiting step.

In contrast, the degradation of 2,4-D during the photochemical reaction using $Fe^{2+}/H_2O_2$ under simulated sunlight irradiation resulted in a carbon isotope shift from −32.0 ± 0.2 ‰ to −26.6 ± 0.3 ‰ at 84.9 % conversion. A carbon isotope effect ($\varepsilon_C = -2.7 \pm 0.2$ ‰) was calculated using Eq. 1 (Figs. 5c and 5d). For the $AKIE_C$ calculation, $n = 8$ and $x = z = 1$ were applied, resulting in a calculated $AKIE_C$ value of 1.021 ± 0.0009.

The $AKIE_C$ value of 1.021 falls within the experimentally derived range for $S_N1$-type nucleophilic substitution (1.00–1.03) [39, 58]. However, it is lower than the $AKIE_C$ values for $S_N2$-type nucleophilic substitution (1.03–1.09) [39, 58, 59] and reductive dechlorination (1.027–1.033) [60]. This indicates that hydrolytic $S_N1$-type nucleophilic substitution was the primary degradation pathway for 2,4-D in the

$Fe^{2+}/H_2O_2$ system under simulated sunlight irradiation. The higher $AKIE_C$ value of 1.021, compared to the $AKIE_C$ value 1.013 for the oxidative cleavage of a C-H bond, partly reflects the fact that the carbon atoms involved in the reaction are now bounded to heavier atoms (e.g., O, Cl) instead of hydrogen. Additionally, the theoretical $AKIE_C$ value for C-Cl bond cleavage is approximately 1.030 [56]. Therefore, the initial cleavage of a C-O bond is identified as the rate-limiting step in this study. Previous studies have demonstrated that during the hydrolysis of MTBE in dilute aqueous acid, the cleavage of the C-O bond from the large tert-butyl group ($(H_3C)_3$-C-O) occurs preferentially over that from the smaller methyl group ($H_3C$-O). The primary carbon isotope effects (1.00–1.03) predicted for this reaction mechanism [24, 27, 39] are comparable to the $AKIE_C$ value observed in the present study. Consequently, the consistent findings between this study and prior research confirm that the cleavage of the C-O bond is the rate-limiting step. Furthermore, the $S_N1$-type nucleophilic substitution serves as the primary reaction mechanism, involving the addition of a proton to the oxygen atom in conjunction with the cleavage of the C-O bond in the $Fe^{2+}/H_2O_2$ system under simulated sunlight irradiation.

*Hydrogen isotope fractionation*: During biodegradation, the hydrogen isotope shifted from $-118 \pm 0$ ‰ to $134 \pm 1$ ‰. A hydrogen isotope effect ($\varepsilon_H = -114.6 \pm 7.9$ ‰), calculated using Eq. 1, was obtained (Figs. 5e and 5f). The apparent kinetic isotope effect for hydrogen ($AKIE_H$) was determined under the assumption that all hydrogen atoms were chemically equivalent and that only hydrogen atoms participated in the reaction, which was considered to occur in a stepwise manner. Therefore, values of $n = 6$, $x = 2$, and $z = 2$ were applied for the calculation of $AKIE_H$. The resulting $AKIE_H$ value was $4.621 \pm 0.0013$. This $AKIE_H$ value (4.621) aligns well with the typical range of hydrogen kinetic isotope effects ($KIE_H$) (2−23) [39] observed during the oxidative cleavage of a C-H bond. This finding indicates that the cleavage of the C-H bond is the dominant rate-limiting step, and significant hydrogen isotope fractionation occurs during biodegradation. Previous studies indicate that the large $AKIE_H$ of 14–23 for the aerobic biodegradation of toluene by *Pseudomonas putida mt-2* confirms that the cleavage of the C-H bond in the methyl group is the rate-limiting step in this reaction [61]. Similar findings were reported by Gray et al. [54], who documented that the addition of fumarate to the toluene methyl group, followed by the breakage of a C-H bond, is the initial step in the anaerobic biodegradation of toluene. This process results in significant hydrogen isotope fractionation of the residual toluene. In this study, along with the initial biodegradation products, the primary $AKIE_H$ suggests that the biodegradation reaction involves the cleavage of a C-H bond in the methylene carbon of the side chain.

For the photochemical reaction involving $Fe^{2+}/H_2O_2$ under simulated sunlight irradiation, the hydrogen isotope shifted from $-117 \pm 1$ ‰ to $-117 \pm 1$ ‰ at 84.9 % conversion. No hydrogen isotope fractionation was observed (Fig. 5e), indicating that the cleavage of the hydrogen bond was not the dominant rate-limiting step. This finding is consistent with the carbon isotope fractionation observed in the photochemical reaction. In the $S_N1$-type nucleophilic substitution reaction mechanism, a C-O bond is broken; therefore, no primary hydrogen isotope effects are expected.

*Chlorine isotope fractionation*: During biodegradation, the $\delta^{37}Cl$ values were determined by GC-qMS and calculated according to Eqs. 3 and 4. The $\delta^{37}Cl$ values for chlorine isotopes shifted from $-3.3 \pm 0.3$ ‰ to $-3.4 \pm 0.3$ ‰, resulting in a $\Delta\delta^{37}Cl$ value of approximately $-0.1 \pm 0.01$ ‰ (Fig. 5a). This change represents a subtle difference that is and close to the confidence interval uncertainties (± 0.2 ‰) [28, 62]. Similarly, no chlorine isotope fractionation was observed in the sterilized control (Fig. S5), confirming that biodegradation did not alter the chlorine isotope composition ($\delta^{37}Cl$) during the experiment. Also, during the photochemical degradation of 2,4-D by $Fe^{2+}/H_2O_2$ under simulated sunlight irradiation, no chlorine isotope fractionation was observed (Fig. 5c). The apparent kinetic isotope effect for chlorine ($AKIE_{Cl}$) values for both biotic and abiotic degradation were measured at 1.000. The Streitweiser limit for C-Cl bond cleavage is 1.013 [28]. Previous studies demonstrate that the $AKIE_{Cl}$ values for chlorinated organic compounds via C-Cl bond cleavage in the initial reaction step are 1.013–1.021 [41] and the $AKIE_{Cl}$ values associated with $S_N2$-type nucleophilic substitution are 1.006–1.009 [63]. Additionally, several laboratory studies report $AKIE_{Cl}$ values for the enzymatic dehalogenation of 1,2-dichloroethane (1.007) [64], as well as for the dechlorination of 1,2-dichloroethane (1.005) and 1-chlorobutane (1.007) catalyzed by haloalkane hydrolytic dehalogenase [65], and for the hydrolysis/dehydrohalogenation of 1,1,1-trichloroethane (1.015) [31]. All the evidence suggests that no C-Cl bond cleavage occurred in the initial reaction step during the biodegradation by *Stenotrophomonas maltophilia* sp. and the photochemical reaction involving $Fe^{2+}/H_2O_2$ under simulated sunlight irradiation.

### 3.6. Mechanistic insights

Based on the identified intermediates and the characteristics of isotope fractionation during various transformation processes, the underlying reactive mechanisms were proposed for the transformation of 2,4-D by *Stenotrophomonas maltophilia* sp. and $Fe^{2+}/H_2O_2$ under simulated sunlight irradiation (Scheme 1).

In the biotransformation process, 2,4-D is enzymatically cleaved by an $\alpha$-ketoglutarate-dependent dioxygenase into 2,4-DCP and glyoxylate. Although glyoxylate has not been isolated as a reaction product, the behavior of the carboxyl and methylene carbons indicates that glyoxylate was indeed formed from the acetate moiety of 2,4-D. However, the fate of the ether-oxygen bond (C-O), whether it is $C_1$'-O or $C_1$-O, may be determined by the measured AKIE values. In this biotransformation, the cleavage of a C-H bond is the dominant rate-limiting step. The reaction under consideration involved the oxidative cleavage of the C-H bond, as observed in both aerobic and anaerobic oxidation of the aromatic methyl group [61]. Protons were activated by both carboxyl and phenoxy groups [8], leading to the prior oxidation of the methylene carbon ($C_1$'). This oxidation occurred through the cleavage of one C-H bond, resulting in the formation of an $\alpha$-hydroxy compound (A) (Scheme 1, route a). The results were consistent with primary carbon and hydrogen isotope fractionation. Subsequently, the ether-oxygen bond ($C_1$'-O) was presumably cleaved, yielding 2,4-DCP and glyoxylate. Later 2,4-DCP was hydroxylated to produce 3,5-dichlorocatechol. Therefore, the oxidation of the C-H bond from the side-chain methylene carbon ($C_1$') was the dominant rate-limiting step in the biotransformation, followed by the cleavage of the $C_1$'-O bond.

In contrast, during the abiotic transformation via $Fe^{2+}/H_2O_2$ under simulated sunlight irradiation, $^{\bullet}OH$ emerged as the primary reactive species, known for their addition reactions to aromatic rings, including benzene and its substituted derivatives [29]. The predominant product formed in this abiotic transformation was 2,4-DCP. No hydroxylated 2,4-D intermediates were identified, and the transition states and small organic acid molecules may not have been detected. Numerous studies on the reaction mechanisms of 2,4-D with $^{\bullet}OH$ have been published in the literatures [21–23, 29, 66]. However, based on the current evidence regarding the intermediates and isotope fractionation characteristics, an underlying reactive mechanism can be inferred (Scheme 1, route b). The initial step involves a rapid pre-equilibrium in which a proton is transferred to the oxygen of the ether, resulting in the formation of the conjugate acid of 2,4-D (B). Subsequently, the transition state (B) was followed by $^{\bullet}OH$-mediated cleavage of the ether-oxygen bond ($C_1$-O), resulting in the formation of the major product 2,4-DCP. The primary $AKIE_C$ and secondary $AKIE_H$ values indicated that the cleavage of the ether-oxygen bond ($C_1$-O) between the aromatic carbon ($C_1$) and the oxygen (O) of the ether was the rate-limiting step, with an $S_N1$-type nucleophilic substitution serving as the underlying reaction mechanism. The degradation of 2,4-D through the formation of a common carbocation intermediate has been supported by previous reaction studies [24, 27, 31]. Subsequently, 2,4-DCP underwent dehalogenation or

hydroxylation to yield 4,6-dichlororesorcinol, 4-chlorophenol, 2-chlorohydroquinone, and phenol. Finally, these intermediates were rapidly oxidized and polymerized into a mixture of polyquinonoid humic acids.

## 4. Conclusions

The present study aimed to investigate the underlying reaction mechanisms of 2,4-D by an indigenous strain of *Stenotrophomonas maltophilia* sp. and $Fe^{2+}/H_2O_2$ under simulated sunlight irradiation, utilizing multiple isotope analysis in an aqueous environment. Based on the identification of transformation products and multiple isotope analysis, H abstraction from the methylene carbon of the side chain, followed the by trapping of the resulting $^{\bullet}OH$ and the cleavage of the ether-oxygen ($C_1$'-O) bond, was identified as the primary reactive pathway for the indigenous strain of *Stenotrophomonas maltophilia* sp. In contrast, for the abiotic transformation by $Fe^{2+}/H_2O_2$ under simulated sunlight irradiation, the initial step involved a rapid pre-equilibrium with a proton, followed by the cleavage of the ether-oxygen bond ($C_1$-O), which was the dominant rate-limiting step. The measured AKIE values were consistent with an $S_N1$-type nucleophilic substitution. Therefore, multiple isotope fractionation patterns may provide valuable insights for characterizing the underlying transformation pathways of 2,4-D in laboratory studies and natural environments.

To characterize the sinks of 2,4-D through multiple isotope analysis, a deeper understanding of isotope fractionation patterns is essential. This includes examining the effects of varying reaction conditions, such as temperature and pH, as well as anaerobic degradation and hydrolysis. Furthermore, future research should focus on comparing $^{\bullet}OH$ oxidation with biodegradation studies, particularly those involving enzyme-catalyzed radical oxidation of 2,4-D. By investigating the variations in isotope compositions across different pathways, we can obtain critical information that will enhance our ability to accurately verify transformation pathways at field sites.

## Environmental implication

2,4-Dichlorophenoxyacetic acid, one of the most important phenoxyalkanoic acid herbicides, has been widely used for controlling broadleaf weeds in wheat, corn, and tobacco crop and non-agricultural soils. Thus, it is frequently detected in soils, surface waters and groundwaters at concentrations ranging from several to hundreds of micrograms per liter. Although 2,4-D has a moderate persistence with relatively short half-lives in soils, it is a potential surface water and groundwater contaminant due to its relatively high-water solubility and low sorption by soils. To protect natural and human food resources, it is therefore important to understand its fate and transformation in environments.

## CRediT authorship contribution statement

**Meicheng Wen:** Funding acquisition, Formal analysis, Conceptualization. **Wanjun Wang:** Visualization, Methodology, Funding acquisition. **Chang Yuan:** Investigation. **Suyun Chen:** Investigation. **Jukun Xiong:** Writing – review & editing, Writing – original draft, Supervision, Project administration, Funding acquisition. **Yongyu Liang:** Writing – original draft, Investigation. **Yingxin Yu:** Validation, Supervision, Resources. **Qinhao Lin:** Funding acquisition, Data curation.

## Declaration of Competing Interest

The authors declare that they have no known competing financial interests or personal relationships that could have appeared to influence the work reported in this paper.

## Acknowledgements

This work was financially supported by the National Natural Science Foundation of China (No. 42177192), the National Key Research and Development Program of China (2024YFC3713201), the Guangdong Basic and Applied Basic Research Foundation (Nos. 2024A1515012492 and 2022A1515010815), and the National Natural Science Foundation of China (Nos. 42377364 and 42377365). There is no conflict of interests.

## Appendix A. Supporting information

Supplementary data associated with this article can be found in the online version at doi:10.1016/j.jhazmat.2025.139885.

## Data availability

The data that has been used is confidential.

## References

[1] Peterson, M.A., McMaster, S.A., Riechers, D.E., Skelton, J., Stahlman, P.W., 2016. 2,4-D past, present, and future: a review. Weed Technol 30, 303–345. https://doi.org/10.1614/wt-d-15-00131.1.
[2] Yang, Z., Xu, X., Dai, M., Wang, L., Shi, X., Guo, R., 2018. Combination of bioaugmentation and biostimulation for remediation of paddy soil contaminated with 2,4-dichlorophenoxyacetic acid. J Hazard Mater 353, 490–495. https://doi.org/10.1016/j.jhazmat.2018.04.052.
[3] Loos, R., Locoro, G., Comero, S., Contini, S., Schwesig, D., Werres, F., et al., 2010. Pan-European survey on the occurrence of selected polar organic persistent pollutants in ground water. Water Res 44, 4115–4126. https://doi.org/10.1016/j.watres.2010.05.032.
[4] White, A.M., Nault, M.E., McMahon, K.D., Remucal, C.K., 2022. Synthesizing laboratory and field experiments to quantify dominant transformation mechanisms of 2,4-dichlorophenoxyacetic acid (2,4-D) in aquatic environments. Environ Sci Technol 56, 10838–10848. https://doi.org/10.1021/acs.est.2c0313210838.
[5] Wilson, R.G., Cheng, H.H., 1976. Breakdown and movement of 2,4-D in the soil under field conditions. Weed Sci 24, 461–466. https://doi.org/10.1017/S0043174500066455.
[6] Fenner, K., Canonica, S., Wackett, L.P., Elsner, M., 2013. Evaluating pesticide degradation in the environment: blind spots and emerging opportunities. Science 341, 752–758. https://doi.org/10.1126/science.1236281.
[7] Qiu, P., Yao, J., Chen, H., Jiang, F., Xie, X., 2016. Enhanced visible-light photocatalytic decomposition of 2,4-dichlorophenoxyacetic acid over $ZnIn_2S_4$/g-$C_3N_4$ photocatalyst. J Hazard Mater 317, 158–168. https://doi.org/10.1016/j.jhazmat.2016.05.069.
[8] Helling, C.S., Bollag, J.M., Dawson, J.E., 1968. Cleavage of ether-oxygen bond in phenoxyacetic acid by an arthrobacter species. J. agricu. Food Chem 16, 538–539.
[9] Evans, W.C., Smith, B.S., Fernley, H.N., Davies, J.I., 1971. Bacterial metabolism of 2,4-dichlorophenoxyacetate. Biochem J 122, 543–551. https://doi.org/10.1042/bj1220543.
[10] Yadav, J.S., Reddy, C.A., 1993. Mineralization of 2,4-dichlorophenoxyacetic acid (2,4-D) and mixtures of 2,4-D and 2,4,5-trichlorophenoxyacetic acid by *phanerochaete chrysosporium*. Appl Environ Microbiol 59, 2904–2908. https://doi.org/10.1128/aem.59.9.2904-2908.1993.
[11] Balajee, S., Mahadevan, A., 1990. Dissimilation of 2,4-dichlorophenoxyacetic acid by azotobacter chroococcum. Xenobiotica; the fate of foreign compounds in biological systems 20, 607–617. https://doi.org/10.3109/00498259009046876.
[12] Huang, X., He, J., Yan, X., Hong, Q., Chen, K., He, Q., et al., 2017. Microbial catabolism of chemical herbicides: microbial resources, metabolic pathways and catabolic genes. Pestic Biochem Phys 143, 272–297. https://doi.org/10.1016/j.pestbp.2016.11.010.
[13] Brucha, G., Aldas-Vargas, A., Ross, Z., Peng, P., Atashgahi, S., Smidt, H., et al., 2021. 2,4-Dichlorophenoxyacetic acid degradation in methanogenic mixed cultures obtained from Brazilian amazonian soil samples. Biodegrad 32, 419–433. https://doi.org/10.1007/s10532-021-09940-3.
[14] Wang, Y., Wu, C., Wang, X., Zhou, S., 2009. The role of humic substances in the anaerobic reductive dechlorination of 2,4-dichlorophenoxyacetic acid by *comamonas koreensis* strain CY0. 1 J Hazard Mater 164, 941–947. https://doi.org/10.1016/j.jhazmat.2008.08.097.
[15] Reitzel, L.A., Tuxen, N., Ledin, A., Bjerg, P.L., 2004. Can degradation products be used as documentation for natural attenuation of phenoxy acids in groundwater. Environ Sci Technol 38, 457–467. https://doi.org/10.1021/es030039e.
[16] Aly, O.M., Faust, S.D., 1964. Herbicides in surface waters, studies on fate of 2, 4-D and ester derivatives in natural surface waters. J Agric Food Chem 12, 541–546.
[17] Vialaton, D., Richard, C., 2002. Phototransformation of aromatic pollutants in solar light: photolysis versus photosensitized reactions under natural water conditions. Aquat Sci 64, 207–215. https://doi.org/10.1007/s00027-002-8068-7.

[18] Arkhipova, M., Tereshchenko, L.Y., Arkhipov, Y.M., 1997. Photooxidative purification of water to remove organochlorine pesticide 2, 4-D (2, 4-dichlorophenoxyacetic acid). Russ J Appl Chem 70, 1930–1935.
[19] Grosby, D.G., Tutass, H.O., 1966. Photodecomposition of 2,4-dichlorophenoxyacetic acid. J Agric Food Chem 14, 596–599.
[20] Wenk, J., von Gunten, U., Canonica, S., 2011. Effect of dissolved organic matter on the transformation of contaminants induced by excited triplet states and the hydroxyl radical. Environ Sci Technol 45, 1334–1340. https://doi.org/10.1021/es102212t.
[21] Peller, J., Wiest, O., Kamat, P.V., 2004. Hydroxyl radical's role in the remediation of a common herbicide, 2,4-dichlorophenoxyacetic acid (2,4-d. J Phys Chem A 108, 10925–10933. https://doi.org/10.1021/jp046450l.
[22] Peller, J., Wiest, O., Kamat, P.V., 2003. Mechanism of hydroxyl radical-induced breakdown of the herbicide 2,4-dichlorophenoxyacetic acid (2,4-D). Chem Eur J 9, 5379–5387. https://doi.org/10.1002/chem.200204469.
[23] Li, X.J., Jenks, W.S., 2000. Isotope studies of photocatalysis: dual mechanisms in the conversion of anisole to phenol. J Am Chem Soc 122, 11864–11870. https://doi.org/10.1021/ja994030h.
[24] Elsner, M., McKelvie, J., Lacrampe Couloume, G., Sherwood-Lollar, B.S., 2007. Insight into methyl tert-butyl ether (MTBE) stable isotope fractionation from abiotic reference experiments. Environ Sci Technol 41, 5693–5700. https://doi.org/10.1021/es070531o.
[25] Palau, J., Yu, R., Mortan, S.H., Shouakar-Stash, O., Rosell, M., Freedman, D.L., et al., 2017. Distinct dual C-C1 isotope fractionation patterns during anaerobic biodegradation of 1,2-dichloroethane: potential to characterize microbial degradation in the field. Environ Sci Technol 51, 2685–2694. https://doi.org/10.1021/acs.est.6b04998.
[26] Wang, G., Liu, Y., Wang, X., Dong, X., Jiang, N., Wang, H., 2022. Application of dual carbon-bromine stable isotope analysis to characterize anaerobic microdegradation mechanisms of PBDEs in wetland bottom-water. Water Res 208. https://doi.org/10.1016/j.watres.2021.117854.
[27] O'Reilly, K.T., Moir, M.E., Taylor, C.D., Smith, C.A., Hyman, M.R., 2001. Hydrolysis of *tert*-butyl methyl ether the (MTBE) in dilute aqueous acid. Environ Sci Technol 35, 3954–3961. https://doi.org/10.1021/es001431k.
[28] Rosell, M., Palau, J., Hatijah Mortan, S., Caminal, G., Soler, A., Shouakar-Stash, O., et al., 2019. Dual carbon - chlorine isotope fractionation during dichloroelimination of 1,1,2-trichloroethane by an enrichment culture containing *Dehalogenimonas* sp. Sci Total Environ 648, 422–429. https://doi.org/10.1016/j.scitotenv.2018.08.071.
[29] Zhang, N., Geronimo, I., Paneth, P., Schindelka, J., Schaefer, T., Herrmann, H., et al., 2016. Analyzing sites of OH radical attack (ring vs. side chain) in oxidation of substituted benzenes via dual stable isotope analysis ($\delta^{13}C$ and $\delta^{2}H$). Sci Total Environ 542, 484–494. https://doi.org/10.1016/j.scitotenv.2015.10.075.
[30] Li, G., Zu, L., Wong, P.K., Hui, X., Lu, Y., Xiong, J., et al., 2012. Biodegradation and detoxification of bisphenol a with one newly-isolated strain bacillus sp. Gzb: kinetics, mechanism and estrogenic transition. Bioresour Technol 114, 224–230. https://doi.org/10.1016/j.biortech.2012.03.067.
[31] Palau, J., Shouakar-Stash, O., Hunkeler, D., 2014. Carbon and chlorine isotope analysis to identify abiotic degradation pathways of 1,1,1-trichloroethane. Environ Sci Technol 48, 14400–14408. https://doi.org/10.1021/es504252z.
[32] Xiong, J., Li, G., Peng, P.A., Gelman, F., Ronen, Z., An, T., 2020. Mechanism investigation and stable isotope change during photochemical degradation of tetrabromobisphenol a (TBBPA) in water under LED White light irradiation. Chemosphere 258. https://doi.org/10.1016/j.chemosphere.2020.127378.
[33] Duling, D.R., 1994. Simulation of multiple isotropic spin-trap EPR spectra. J Magn Reson Ser B 104, 105–110. https://doi.org/10.1006/jmrb.1994.1062.
[34] Renpenning, J., Kuemmel, S., Hitzfeld, K.L., Schimmelmann, A., Gehre, M., 2015. Compound-specific hydrogen isotope analysis of heteroatom-bearing compounds via gas chromatography-chromium-based high-temperature conversion (Cr/HTC)-isotope ratio mass spectrometry. Anal Chem 87, 9443–9450. https://doi.org/10.1021/acs.analchem.5b02475.
[35] Hitzfeld, K.L., Gehre, M., Richnow, H.H., 2011. A novel online approach to the determination of isotopic ratios for organically bound chlorine, bromine and sulphur. Rapid Commun Mass Spectrom 25, 3114–3122. https://doi.org/10.1002/rcm.5203.
[36] Ponsin, V., Torrentó, C., Lihl, C., Elsner, M., Hunkeler, D., 2019. Compound-specific chlorine isotope analysis of the herbicides atrazine, acetochlor, and metolachlor. Anal Chem 91, 14290–14298. https://doi.org/10.1021/acs.analchem.9b02497.
[37] Hartenbach, A.E., Hofstetter, T.B., Tentscher, P.R., Canonica, S., Berg, M., Schwarzenbach, R.P., 2008. Carbon, hydrogen, and nitrogen isotope fractionation during light-induced transformations of atrazine. Environ Sci Technol 42, 7751–7756. https://doi.org/10.1021/es800356h.
[38] Lihl, C., Renpenning, J., Kuemmel, S., Gelman, F., Schuerner, H.K.V., Daubmeier, M., et al., 2019. Toward improved accuracy in chlorine isotope analysis: synthesis routes for in-house standards and characterization via complementary mass spectrometry methods. Anal Chem 91, 12290–12297. https://doi.org/10.1021/acs.analchem.9b02463.
[39] Elsner, M., Zwank, L., Hunkeler, D., Schwarzenbach, R.P., 2005. A new concept linking observable stable isotope fractionation to transformation pathways of organic pollutants. Environ Sci Technol 39, 6896–6916. https://doi.org/10.1021/es0504587.
[40] Elsner, M., 2010. Stable isotope fractionation to investigate natural transformation mechanisms of organic contaminants: principles, prospects and limitations. J Environ Monit 12, 2005–2031. https://doi.org/10.1039/c0em00277a.
[41] Palau, J., Cretnik, S., Shouakar-Stash, O., Hoeche, M., Elsner, M., Hunkeler, D., 2014. C and cl isotope fractionation of 1,2-dichloroethane displays unique $\delta^{13}C$ $\delta^{37}Cl$ patterns for pathway identification and reveals surprising C-Cl bond involvement in microbial oxidation. Environ Sci Technol 48, 9430–9437. https://doi.org/10.1021/es5031917.
[42] Sakaguchi-Soeder, K., Jager, J., Grund, H., Matthaeus, F., Schueth, C., 2007. Monitoring and evaluation of dechlorination processes using compound-specific chlorine isotope analysis. Rapid Commun Mass Spectrom 21, 3077–3084. https://doi.org/10.1002/rcm.3170.
[43] Jin, B., Laskov, C., Rolle, M., Haderlein, S.B., 2011. Chlorine isotope analysis of organic contaminants using GC-qMS: method optimization and comparison of different evaluation schemes. Environ Sci Technol 45, 5279–5286. https://doi.org/10.1021/es200749d.
[44] Aeppli, C., Holmstrand, H., Andersson, P., Gustafsson, O., 2010. Direct Compound-specific stable chlorine isotope analysis of organic compounds with quadrupole GC/MS using standard isotope bracketing. Anal Chem 82, 420–426. https://doi.org/10.1021/ac902445f.
[45] Chen, Z.H., Yin, H., Peng, H., Lu, G.N., Liu, Z.H., Dang, Z., 2019. Identification of novel pathways for biotransformation of tetrabromobisphenol a by *Phanerochaete chrysosporium*, combined with mechanism analysis at proteome level. Sci Total Environ 659, 1352–1361. https://doi.org/10.1016/j.scitotenv.2018.12.446.
[46] Wu, X.M., Zhang, C., An, H.M., Li, M., Pan, X.L., Dong, F.S., et al., 2021. Biological removal of deltamethrin in contaminated water, soils and vegetables by *Stenotrophomonas maltophilia*. Chemosphere 279 (10), XQ08. https://doi.org/10.1016/j.chemosphere.2021.130622.
[47] Tan, Z.W., Yang, X.Y., Chen, L., Liu, Y.L., Xu, H.J., Li, Y.T., et al., 2022. Biodegradation mechanism of chloramphenicol by *aeromonas media* SZW3 and genome analysis. Bioresour Technol 344, 10. https://doi.org/10.1016/j.biortech.2021.126280.
[48] Tang, S.Y., Yin, H., Yu, X.L., Chen, S.N., Lu, G.N., Dang, Z., 2021. Transcriptome profiling of *Pseudomonas aeruginosa* YH reveals mechanisms of 2, 2′, 4, 4′-tetrabrominated diphenyl ether tolerance and biotransformation. J Hazard Mater 403, 10. https://doi.org/10.1016/j.jhazmat.2020.124038.
[49] Cao, Y., Yin, H., Peng, H., Tang, S., Lu, G., Dang, Z., 2017. Biodegradation of 2,2′,4,4′-tetrabromodiphenyl ether (BDE-47) by *Phanerochaete chrysosporium* in the presence of $Cd^{2+}$. -11424 Environ Sci Pollut Res 24, 11415. https://doi.org/10.1007/s11356-017-8763-5.
[50] Lin, S.Q., Wei, J.C., Yang, B.T., Zhang, M., Zhuo, R., 2022. Bioremediation of organic pollutants by White rot fungal cytochrome P450: the role and mechanism of CYP450 in biodegradation. Chemosphere 301, 13. https://doi.org/10.1016/j.chemosphere.2022.134776.
[51] Wu, X.W., Wang, W.B., Liu, J.W., Pan, D.D., Tu, X.H., Lv, P., et al., 2017. Rapid biodegradation of the herbicide 2,4-dichlorophenoxyacetic acid by *Cupriavidus gilardii* T-1. J Agric Food Chem 65, 3711–3720. https://doi.org/10.1021/acs.jafc.7b00544.
[52] Liu, F., Zhang, G., Lian, X., Fu, Y., Lin, Q., Yang, Y., et al., 2022. Influence of meteorological parameters and oxidizing capacity on characteristics of airborne particulate amines in an urban area of the pearl river delta, China. Environ Res 212. https://doi.org/10.1016/j.envres.2022.113212.
[53] Ensing, B., Buda, F., Blöchl, P., Baerends, E.J., 2001. Chemical involvement of solvent water molecules in elementary steps of the fenton oxidation reaction. Angew Chem Int Ed 40, 2893–2895. https://doi.org/10.1002/1521-3773(20010803)40:15.
[54] Gray, J.R., Lacrampe-Couloume, G., Gandhi, D., Scow, K.M., Wilson, R.D., Mackay, D.M., et al., 2002. Carbon and hydrogen isotopic fractionation during biodegradation of methyl tert-butyl ether. Environ Sci Technol 36, 1931–1938. https://doi.org/10.1021/es011135n.
[55] Sherwood-Lollar, B.S., Hirschorn, S., Mundle, S.O.C., Grostern, A., Edwards, E.A., Lacrampe-Couloume, G., 2010. Insights into enzyme kinetics of chloroethane biodegradation using compound specific stable isotopes. Environ Sci Technol 44, 7498–7503. https://doi.org/10.1021/es101330r.
[56] Liang, X., Howlett, M.R., Nelson, J.L., Grant, G., Dworatzek, S., Lacrampe-Couloume, G., et al., 2011. Pathway-dependent isotope fractionation during aerobic and anaerobic degradation of monochlorobenzene and 1,2,4-trichlorobenzene. Environ Sci Technol 45, 8321–8327. https://doi.org/10.1021/es201224x.
[57] Nijenhuis, I., Andert, J., Beck, K., Kästner, M., Diekert, G., Richnow, H.H., 2005. Stable isotope fractionation of tetrachloroethene during reductive dechlorination by sulfurospirillum multivorans and desulfitobacterium sp strain PCE-S and abiotic reactions with cyanocobalamin. Appl Environ Microbiol 71, 3413–3419. https://doi.org/10.1128/aem.71.7.3413-3419.2005.
[58] Elsayed, O.F., Maillard, E., Vuilleumier, S., Nijenhuis, I., Richnow, H.H., Imfeld, G., 2014. Using compound-specific isotope analysis to assess the degradation of chloroacetanilide herbicides in lab-scale wetlands. Chemosphere 99, 89–95. https://doi.org/10.1016/j.chemosphere.2013.10.027.
[59] Droz, B., Drouin, G., Maurer, L., Villette, C., Payraudeau, S., Imfeld, G., 2021. Phase transfer and biodegradation of pesticides in water-sediment systems explored by compound-specific isotope analysis and conceptual modeling. Environ Sci Technol 55, 4720–4728. https://doi.org/10.1021/acs.est.0c06283.
[60] Helbling, D.E., Hollender, J., Kohler, H.P.E., Fenner, K., 2010. Structure-based interpretation of biotransformation pathways of amide-containing compounds in sludge-seeded bioreactors. Environ Sci Technol 44, 6628–6635. https://doi.org/10.1021/es101035b.
[61] Morasch, B., Richnow, H.H., Schink, B., Meckenstock, R.U., 2001. Stable hydrogen and carbon isotope fractionation during microbial toluene degradation:

mechanistic and environmental aspects. Appl Environ Microbiol 67, 4842–4849. https://doi.org/10.1128/aem.67.10.4842-4849.2001.
[62] Yu, X., Yin, H., Peng, H., Lu, G., Liu, Z., Li, H., et al., 2020. Degradation mechanism, intermediates and toxicology assessment of tris-(2-chloroisopropyl) phosphate using ultraviolet activated hydrogen peroxide. Chemosphere 241. https://doi.org/10.1016/j.chemosphere.2019.124991.
[63] Swiderek, K., Paneth, P., 2012. Extending limits of chlorine kinetic isotope effects. J Org Chem 77, 5120–5124. https://doi.org/10.1021/jo300682f.
[64] Lewandowicz, A., Rudzinski, J., Tronstad, L., Widersten, M., Ryberg, P., Matsson, O., et al., 2001. Chlorine kinetic isotope effects on the haloalkane dehalogenase reaction. J Am Chem Soc 123, 4550–4555. https://doi.org/10.1021/ja003503d.
[65] Holt, B.D., Sturchio, N.C., Abrajano, T.A., Heraty, L.J., 1997. Conversion of chlorinated volatile organic compounds to carbon dioxide and methyl chloride for isotopic analysis of carbon and chlorine. Anal Chem 69, 2727–2733. https://doi.org/10.1021/ac961096b.
[66] Zepp, R.G., Wolfe, N.L., Gordon, J.A., Baughman, G.L., 1975. Dynamics of 2,4-D esters in surface waters, hydrolysis, photolysis, and vaporization. Environ Sci Technol 9, 1144–1150. https://doi.org/10.1021/es60111a001.